Experimental Characterization of a Deployed Early-Warning System for SOP-Based Monitoring of Debris Flows in Mountain Scenarios

Experimental Characterization of a Deployed Early-Warning System for SOP-Based Monitoring of Debris Flows in Mountain Scenarios

1st Saverio Pellegrini
Politecnico di Torino
DET, Torino, Italy
saverio.pellegrini@polito.it

2nd Dhia El Hak Daamouche
Politecnico di Torino
DET, Torino, Italy
dhiaelhak.daamouche@studenti.polito.it

3rd Roberto Gaudino
Politecnico di Torino
DET, Torino, Italy
roberto.gaudino@polito.it

4th Giuseppe Rizzelli
Politecnico di Torino
Photonext Center, Torino, Italy
giuseppe.rizzelli@polito.it

***Abstract*—We present an in-field experimental characterization of the detection capabilities of an installed prototypical interrogator for optical fiber-based real-time monitoring of a real mountain gully.**

***Index Terms*—mountain engineering, fibers, polarization sensing, debris flow**

I. Introduction

The mountain environment is subject to dangerous and highly disruptive events, possibly harming people and infrastructures integrity. Different solutions are employed to provide early warnings of hazards: standard ones used in mountain engineering include geophones, seismometers, [1]–[3], or other fully mechanical solutions (wires, inclinometers) [4] able to detect flowing masses. Main limitations concern their non distributed, but discrete, nature, which could sometimes generate unreliable warnings. Radar or camera-based systems [5] are also employed, with the limits of needing an in situ power supply (which could be damaged during the event occurrences) and limited capabilities in reduced visibility conditions. Rain gauges [3] could be of help to detect initiating conditions but cannot provide precise and timely warnings.

On the other side, optical fiber-based early warning systems have been widely studied and employed in several scenarios to both locate and detect mechanical stresses and vibrations. Distributed techniques based on Brillouin or Rayleigh light backscattering [6]–[8] or interferometric techniques [9], [10] have been largely used in these contexts. Their complexity and need for expensive hardware make it difficult, nonetheless, to install them in the mountain scenario.

The monitoring of the state of polarization (SOP) [11] has been also discussed as a method to detect vibrational events connected to hazards, and its reliability has recently been tested for earthquakes, intrusions, and hazard detection [12], [13]. The need for much cheaper hardware could suit the needs of implementing this technique in the mountain environment, at the cost of the unavailability to localize events. The latter, in these scenarios, could be of secondary importance, even if rough events positioning, along with speed estimation, could be in principle delivered [14]. In this paper, we delve into the characterization of an optical fiber polarization-based system, able to deliver, in principle, timely early warnings. This very same system has been previously discussed in our works [14], [15]. Noise and simulated events will be addressed to deliver a first characterization of the detection capabilities.

979-8-3315-9777-1/25/$31.00 ©2025 IEEE

II. Experimental Setup and Processing Algorithm

The experimental testbed shown in Fig. 1(a) concerns a real installation in a mountain environment. It's important to underline that the gully is active, and flowing mass events, such as debris flows, occur at least once a year, posing a particular risk to the roadway below. Four fiber circuits (shown in photos with different colors in Fig. 1a-b) are installed throughout the length of the gully, mostly transversely. Circuit #1 (in orange in Fig. 1a), is longitudinally installed along the gully. This optical fiber circuit is reported for completeness, but it is not active at the moment. Circuit #2 (in purple in Fig. 1a) is not buried but installed on the vertical side of an artificial dam-like structure, a weir. Circuit #3 (in green in Fig. 1a) is buried in between Circuit #4 and Circuit #2, at about 30 meter distance from both of them. Circuit #4 (in red in Fig. 1a) is positioned at a 40-meter distance from the main road, buried a few centimeters below the soil surface. The blue line in Fig. 1a is the common multi-fiber cable, carrying the optical fiber circuits on the common path along the gully length. Each circuit is connected to a pair of fibers inside the multi-fiber cable that carry the optical signal from the laser (upstream direction) and back to the polarimeter (downstream direction) in a loop-back configuration. A total of eight fibers of the multi-fiber cable are thus used. The system comprises solar panels to supply the interrogator, where all the necessary hardware is positioned. As depicted in Fig. 1a, the interrogator and solar panels are placed in safe positions on the higher sides of the gully, where rockfall events cannot damage them. The gully is about 3 to 5 meters deep, depending on the altitude. Fig. 1b shows the main components of the interrogator hardware. The same optical signal is fed in upstream to all the four circuits through a 1x4 optical splitter. In downstream, the circuit to be monitored is selected through an optical switch placed at the polarimeter

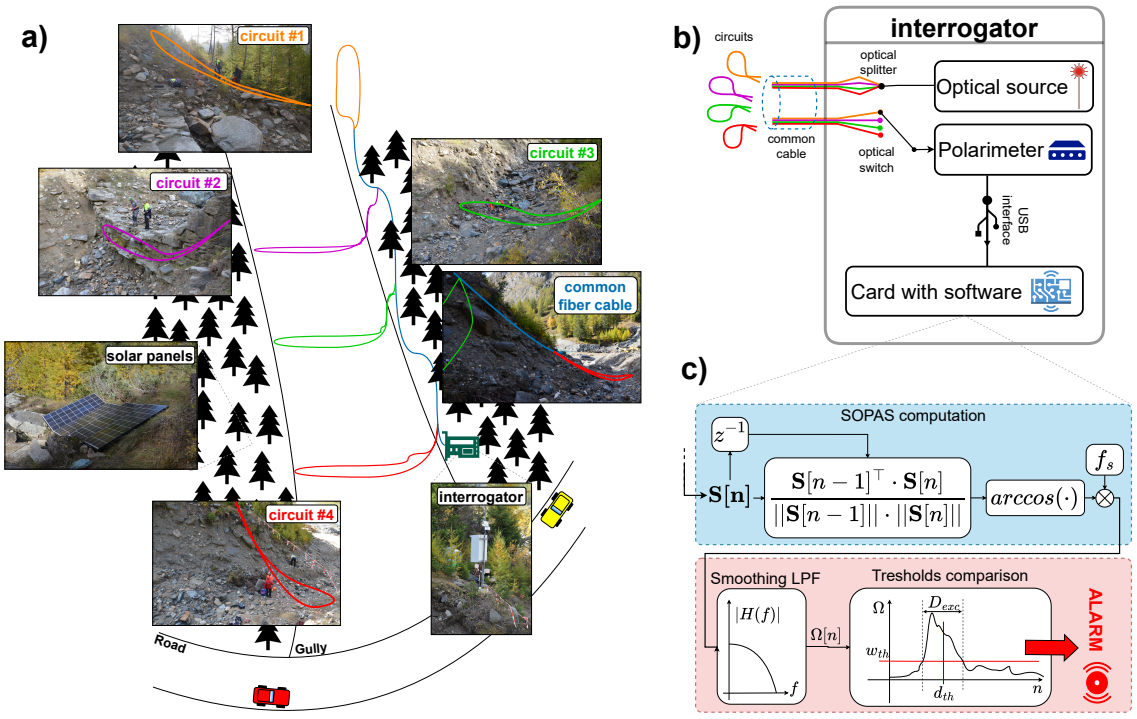

Fig. 1. (a) Experimental setup of the monitored gully, including photos of the actual fiber installations, interrogator, and solar panels. Red, green, purple, yellow, and blue lines refer to circuits #4, #3, #2, #1, and common fiber cable. (b) Simplified interrogator scheme. (c) Proposed processing and alarming algorithm running in the card connected to the polarimeter.

input. The total length of each circuit ranges from 200 m for Circuit #4 to 400 m for Circuit #1. The laser launch power is 17 dBm, whereas the received power is above -4 dBm for each circuit. The interrogator is placed over a pole fixed to the ground by a set of iron strings for enhanced robustness to weather-induced spurious vibrations. The interrogator box is temperature-controlled and water-resistant. Besides the optical devices, the box contains all the necessary hardware for data transmission to an outside server and for alarm communication to a pair of traffic lights on the road. The sampling frequency of the system is f_s =100 Hz, and samples represent the SOP angular speed (SOPAS) Ω, defined in the light-blue rectangle in Fig. 1c. This parameter describes the angular speed at which the SOP moves over the Poincaré sphere and is strictly related to the intensity of vibrations occurring on the fiber [14]–[16]. It is computed from consecutive Stokes vectors $\mathbf{S}[n]$ (where n is the discrete time index) time evolution. The red rectangle describes a proposed algorithm to deliver alarms based on thresholds. After filtering (simple moving average filter, with window fixed to 100 samples, i.e. 1 second), the $\Omega[n]$ time evolution is compared to:

- SOPAS threshold ω_{th}, over the $\Omega[n]$ signal which may exceed it if a potentially hazardous vibrational event is detected by the fiber circuit under test.
- Time threshold d_{th}, on the duration. Whenever the SOPAS exceeds ω_{th}, it remains above threshold for a time D_{exc}, as specified in Fig. 1c. If this duration exceeds the d_{th} time threshold, the occurrence is classified as a dangerous event, and an alarm is triggered. In fact, dangerous flowing mass events have a bursty behavior, where each burst lasts tens of seconds, whereas false alarms are anomalies with a much shorter duration.

In this work, since no real dangerous event has been recorded, each time the conditions $\Omega[n] \geq \omega_{th}$ is satisfied together with $D_{exc} \geq d_{th}$, we will refer to exceedances happening. Consequently, each time an exceedance is recorded for a specific pair of ω_{th} and d_{th}, the system is subject to false alarms. The goal of this paper is then to find the optimal system working condition so that the false alarm occurrences could be minimized. The choice of d_{th} is critical to deliver timely alarms, and should be kept low. In the following, it will be kept below 2 seconds, so that the alarm would be triggered at most two seconds after the SOPAS threshold exceedance, which is also affected by the time average window length.

III. Data Analysis and Discussion

Starting in late November 2024 we recorded SOPAS samples from the different circuits. Since noise, intended as anything not related to dangerous events but that couples to the fibers and makes the SOPAS change, is dependent on external conditions and fibers displacements, this paper reports an interesting case study for 12 straight hours, acquired at different times for circuits #2, #3, and #4. Since parallel

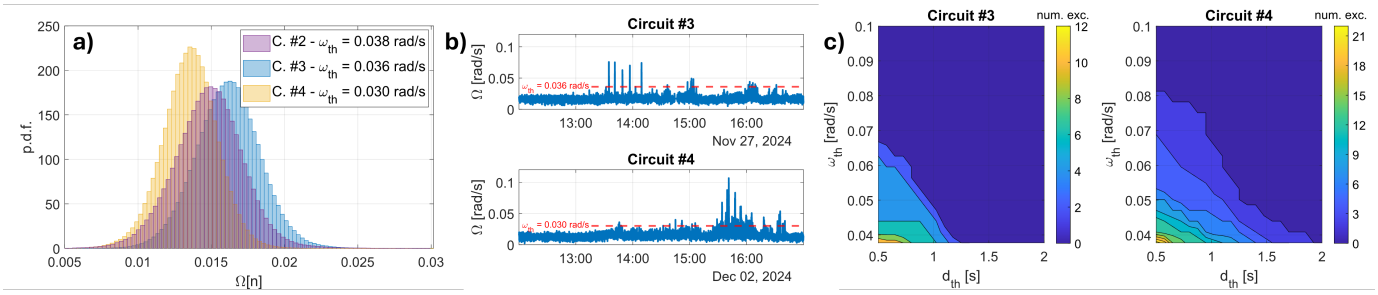

Fig. 2. (a) pdfs of consecutive 12 hours acquired, per circuit. (b) SOPAS evolution recorded during anomalous noisy hours for circuits #3 and #4. (c) Exceedances detection maps for circuits #3 and #4.

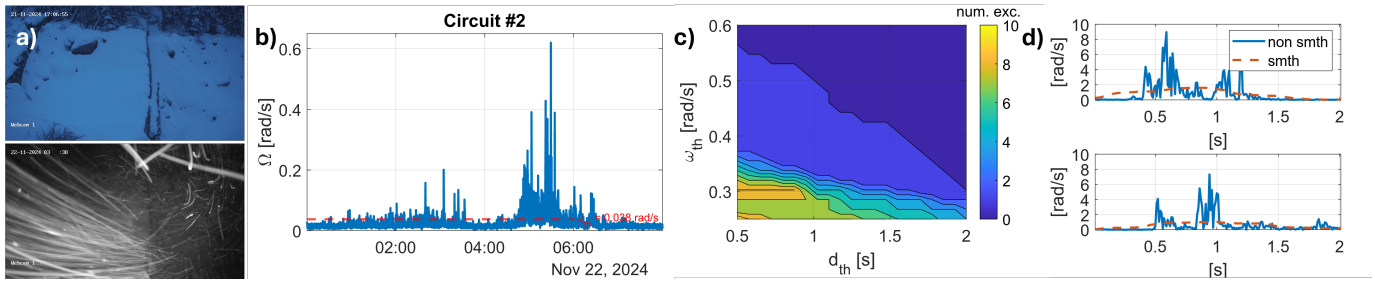

Fig. 3. (a) upper photo shows the gully on circuit #2 with a snow layer in quiet conditions, lower photo shows the occurrence of an intense snowfall on the same spot. (b) SOPAS evolution recorded on circuit #2 during an intense snowfall. (c) Exceedences detection map for circuit #2. (d) Simulated flowing mass event response on SOPAS, non-smoothed (blue line, "no smth") and smoothed (orange dashed line, "smth").

monitoring is not yet available, samples were acquired from 23-11-24 00:00 for circuit #2, 27-11-24 00:00 for circuit #3, and 30-11-24 12:00 for circuit #4. Around November 20th, after a snowfall, the monitored gully was covered by a thick layer of ice and snow. This scenario is quite common since temperatures in the area can reach about $-10°$C. Fig. 2a shows the probability density functions (pdfs) of the recorded, time-averaged, SOPAS samples in the 12-hour time window. The three distributions depict a very stable and comparable noise level between the circuits, with very few outliers: more than 99.9% of the SOPAS samples lie below 0.03 rad/s for all of them. This confirms a quite steady behavior of the SOP when ice covers the gully, as expected. Defining $P_{99.9\%}$ as the 99.9th percentile of the distributions in Fig. 2a, as a general rule of thumb, the detection threshold on the SOPAS values is fixed to $\omega_{th} = 1.5 \cdot P_{99.9\%}$, with the values per circuit shown in the legend. With these thresholds, the recorded time when $\Omega[n] \geq \omega_{th}$ is in between 0 and 2 seconds, depending on the selected circuit. Focusing now on circuits #3 and #4, which are both buried, no noticeable variations were recorded in the presence of strong snowfalls, which occurred several times in the days before and after the acquisitions, making us infer some insensitivity to this kind of event. The only noticeable anomalies are depicted in Fig. 2b, where the SOPAS exceeds ω_{th} for tens of seconds for circuit #3 and almost one hour for circuit #4. We underline that this behavior is difficult to relate to any known external condition, as rainfall, snowfalls, or animal activity in the gully (which has been recorded several times by cameras). However, it strongly characterizes the noise level of these two circuits. In this case, a simple fixed threshold on SOPAS value is less effective, as it would lead to false alarms for several minutes, which is hardly acceptable. As discussed above, introducing a second threshold on the exceedances duration D_{exc}, could enhance the detection performances. In Figure 2c, two detection maps for the two circuits #3 and #4 show the number of exceedances per ω_{th} and d_{th} parameters pair, considering the whole 12 hours dataset used for the pdfs in Fig. 2a, where no anomalous behavior is recorded, and the SOPAS behavior in Fig. 2(b). For low threshold values, the majority of exceedances has short duration ($D_{exc} \leq d_{th}$), whereas the trend is inverted when the threshold is increased. This is reasonable since a small ω_{th} leads to take into account short noise peaks, oscillating around the threshold. This is confirmed by the majority of exceedances being below $d_{th} = 0.5$ seconds. The maps show that, for circuit #3, to eliminate false alarms any ω_{th} value can be selected provided that d_{th} is larger than about 1.3 seconds. This leads to exactly 0 exceedances (i.e. 0 false alarms). For circuit #4, the background noise level is slightly higher, but more than half of the parameter pairs in the map could lead to the no false alarms condition. Although this is not exhaustive since only 24 hours in total have been studied, it gives a comprehensive idea of the working principle and performances of the system. Actual performance evaluation with real-life events will give a more complete idea of the actual detection performances of these two circuits. Through the years, several sensors have been installed in this gully and recorded the occurrences of actual hazardous flowing masses:

the recorded duration is much longer than the one shown in the maps, with much higher intensity, realistically leading to much higher SOPAS values.

In circuit #2, the situation is quite different. This fiber cable is not buried, but completely exposed, fixed on the dam-like weir structure. Fig. 1a shows the fiber displacement as seen by the front, without snow, while Fig. 3a, upper photo, shows the same structure as seen from above and with snow. In the same Figure, the photo below shows the occurrence of a very intense snowfall, generating the SOPAS variations reported in Fig. 3b. Unlike the other buried circuits, circuit #2 is extremely sensitive to external weather conditions: a threshold value of 0.038 rad/s, delivering 0 seconds of false alarm in the 12 hours recorded to generate the pdfs in Fig. 2a, is now too low and completely immersed in noise, generating hours of alarms. The detection scenario in this case changes completely: even with d_{th} values near to 2 seconds, with ω_{th} around 0.038 rad/s, the number of exceedances never reaches 0, and decreases, with increasing duration thresholds to a few tens at most. In order to reach a number of exceedances and a map layout similar to the ones of circuits #3 and #4, the SOPAS threshold values need to be increased in the range from 0.2 rad/s, to 0.6 rad/s as shown in Fig. 3c, that is one order of magnitude larger. This is due to the very different layout and installation of this fiber circuit. Moreover, being exposed the fiber is more subject to the effect of flowing masses, to which the buried circuits are less sensitive. In order to characterize the effect of a flowing mass on this circuit, we tested the fall of gravel and sand on the fiber. The results are reported in Fig. 3d, for two occurrences. The blue curve shows the original SOPAS trace, while the orange dashed line shows the time-averaged trace, with Ω values up to 2 rad/s in correspondence of the event. An actual flowing mass would hit the fiber continuously for much longer than two seconds [17]. These events have been recorded at least once a year in this gully, occurring in bursts of tens of seconds. As such they would produce time-averaged SOPAS values much longer and much larger than the 1-2 rad/s measured during our tests. Considering the map in Fig. 3c then, a threshold value with ω_{th} being in between 0.4-0.5 rad/s and $d_{th} > 1.2$ seconds, would allow for consistent detection performances reducing the number of false alarm due to external intense snowfall, as shown by the recorded data.

IV. Conclusions

This paper introduces a quite unique SOP-fiber-based detection system installed in a mountain environment over an active gully subject to intense and dangerous flowing masses. Preliminary data analysis shows interesting consequences on the SOPAS due to the external environment, which nevertheless seems to be not critical for the detection performances of the system. Despite having different circuits with different noise characteristics, a simple intensity ω_{th} and duration d_{th} threshold can deliver good detection performances and resilience to false alarm occurrences. The results reported in this work are nevertheless still preliminary: a distributed study over several months is necessary, as well as characterization of truly dangerous events occurrences.

Acknowledgment

The work was partially supported by SURENET project – funded by European Union – Next Generation EU within the PRIN 2022 program (D.D. 104 - 02/02/2022 Ministero dell'Universit'a e della Ricerca). This manuscript reflects only the authors' views and opinions and the Ministry cannot be considered responsible for them.

References

[1] M. Arattano and L. Marchi, "Systems and Sensors for Debris-flow Monitoring and Warning," *Sensors*, vol. 8, no. 4, pp. 2436–2452, 2008.

[2] S.-C. Wei and K.-F. Liu, "Automatic debris flow detection using geophones," *Landslides*, vol. 17, no. 2, pp. 349–359, 2020.

[3] M. Hürlimann, V. Coviello, C. Bel, X. Guo, M. Berti, C. Graf, J. Hübl, S. Miyata, J. B. Smith, and H.-Y. Yin, "Debris-flow monitoring and warning: Review and examples," *Earth-Science Reviews*, vol. 199, p. 102981, 2019.

[4] F. Antolini, S. Aiassa, and M. Barla, "An early warning system for debris flows and snow avalanches," in *Geotechnical Research for Land Protection and Development*, pp. 338–347, Springer International Publishing, 2020.

[5] M. Barla and F. Antolini, "An integrated methodology for landslides' early warning systems," *Landslides*, vol. 17, no. 2, pp. 215–228, 2016.

[6] L. B. Liokumovich, N. A. Ushakov, O. I. Kotov, M. A. Bisyarin, and A. H. Hartog, "Fundamentals of Optical Fiber Sensing Schemes Based on Coherent Optical Time Domain Reflectometry: Signal Model Under Static Fiber Conditions," *Journal of Lightwave Technology*, vol. 33, no. 17, pp. 3660–3671, 2015.

[7] E. F. Williams, M. R. Fernández-Ruiz, R. Magalhaes, R. Vanthillo, Z. Zhan, M. González-Herráez, and H. F. Martins, "Distributed sensing of microseisms and teleseisms with submarine dark fibers," *Nature Communications*, vol. 10, 2019.

[8] Y. Muanenda, C. J. Oton, and F. Di Pasquale, "Application of Raman and Brillouin Scattering Phenomena in Distributed Optical Fiber Sensing," *Frontiers in Physics*, vol. Volume 7 - 2019, 2019.

[9] I. Di Luch, M. Ferrario, G. Rizzelli, R. Gaudino, and P. Boffi, "Vibration sensing for deployed metropolitan fiber infrastructures," in *Optical Fiber Communications Conference and Exhibition*, pp. 1–3, IEEE, 2020.

[10] I. DI Luch, P. Boffi, M. Ferrario, G. Rizzelli, R. Gaudino, and M. Martinelli, "Vibration Sensing for Deployed Metropolitan Fiber Infrastructure," *Journal of Lightwave Technology*, vol. 39, no. 4, pp. 1204–1211, 2021.

[11] L. Palmieri and A. Galtarossa, "Coupling Effects Among Degenerate Modes in Multimode Optical Fibers," *IEEE Photonics Journal*, vol. 6, no. 6, pp. 1–8, 2014.

[12] A. Mecozzi, C. Antonelli, M. Mazur, N. Fontaine, H. Chen, L. Dallachiesa, and R. Ryf, "Use of Optical Coherent Detection for Environmental Sensing," *Journal of Lightwave Technology*, vol. 41, no. 11, pp. 3350–3357, 2023.

[13] A. Mecozzi, M. Cantono, J. C. Castellanos, V. Kamalov, R. Muller, and Z. Zhan, "Polarization sensing using submarine optical cables," *Optica*, vol. 8, pp. 788–795, Jun 2021.

[14] S. Pellegrini, G. Rizzelli, M. Barla, and R. Gaudino, "Polarization-Based Fiber Optic System for Debris Flow Early Warning: On-Field Demonstration," *IEEE Photonics Journal*, vol. 16, no. 3, pp. 1–8, 2024.

[15] S. Pellegrini, G. Rizzelli, M. Barla, and R. Gaudino, "Algorithm Optimization for Rockfalls Alarm System Based on Fiber Polarization Sensing," *IEEE Photonics Journal*, vol. 15, no. 3, pp. 1–9, 2023.

[16] S. Pellegrini, L. Minelli, L. Andrenacci, G. Rizzelli, D. Pilori, G. Bosco, L. D. Chiesa, C. Crognale, S. Piciaccia, and R. Gaudino, "Overview on the state of polarization sensing: application scenarios and anomaly detection algorithms," *J. Opt. Commun. Netw.*, vol. 17, pp. A196–A209, Feb 2025.

[17] V. Coviello, M. Arattano, F. Comiti, P. Macconi, and L. Marchi, "Seismic Characterization of Debris Flows: Insights into Energy Radiation and Implications for Warning," *Journal of Geophysical Research: Earth Surface*, vol. 124, no. 6, pp. 1440–1463, 2019.